Comput Mech (2009) 44:297–307
DOI 10.1007/s00466-009-0371-x

ORIGINAL PAPER

# Multi-scale homogenization of moving interface problems with flux jumps: application to solidification

**Sangmin Lee · Veera Sundararaghavan**

Received: 1 October 2008 / Accepted: 21 January 2009 / Published online: 20 February 2009


**Abstract** In this paper, a multi-scale analysis scheme for solidification based on two-scale computational homogenization is discussed. Solidification problems involve evolution of surfaces coupled with flux jump boundary conditions across interfaces. We provide consistent macro-micro transition and averaging rules based on Hill's macro-homogeneity condition. The overall macro-scale behavior is analyzed with solidification at the micro-scale modeled using an enthalpy formulation. The method is versatile in the sense that two different models can be employed at the macro- and micro-scales. The micro-scale model can incorporate all the physics associated with solidification including moving interfaces and flux discontinuities, while the macro-scale model needs to only model thermal conduction using continuous (homogenized) fields. The convergence behavior of the tightly coupled macro-micro finite element scheme with respect to decreasing element size is analyzed by comparing with a known analytical solution of the Stefan problem.

**Keywords** Multi-scale modeling · Interface evolution · Homogenization · Solidification

## 1 Introduction

Solidification is inherently multi-scale in nature. Interaction between thousands of crystals gives the overall behavior of the solidification process and defines the properties of the final product. Investigating the interaction and growth of crystals in the micro-scale is computationally very intensive, whereas macro-scale models lack accuracy being based on a large number of simplifications. Multi-scale modeling by coupling macroscopic and microscopic models allow us to take advantage of both the efficiency of the macroscopic models and the accuracy of the microscopic models. Multi-scale analysis of general heat conduction problems have been previously addressed using micro-scale effective properties obtained through either bounding relations [1,2] or analytical closed-form expressions (reviewed in [3]) in a macro-scale model. These approaches were restricted to simple geometries with a simple material response, not yielding accurate results when discontinuous interfaces are present. More recently, numerical schemes using asymptotic homogenization approaches, based on an expansion of the unknown temperature or displacement with respect to a micro-scale length parameter, have been developed to address micro-macro heat conduction problems [4–9]. However, the problems considered are restricted to constant conductivity and focused on steady-state heat conduction problems. Solidification problems involve transient effects, and in addition, field discontinuities (flux jumps) that have not been previously addressed in a multi-scale methodology. Previous works in literature for addressing multi-scale solidification problems have involved analytical studies [10] or simple numerical computation [11] at the micro-scale followed by transfer of data to the macro-scale model. Other approaches include multi-scale algorithms driven by microscopic numerical solution data, e.g., database look-up or regression fit [12,13] and sub-grid modeling [14] approaches. A recent article in this journal summarizes various techniques proposed in the solid and fluid mechanics community for addressing multi-scale problems in general [15].

In [10], the macroscopic transport equations are derived using volume averaging technique and closed by supplementary relations, which are obtained from the micro-scale. In [10], there is no numerical computation performed at the

S. Lee · V. Sundararaghavan (✉)
Department of Aerospace Engineering,
University of Michigan, Ann Arbor, MI 48109, USA
e-mail: veeras@umich.edu

micro-scale. In [12,13], micro-scale computations are used to obtain data for regression fit of a predictive equation, which is further used for macro-scale computation. Since micro- and macro-scale equations are decoupled in database approaches, they do not model loading history dependence and non-linearity in micro-scale data. In [11], microscopic modeling is done by assuming periodic distribution of crystals and numerical computation of a single crystal growth is carried out for every point of a macroscopic grid to provide information for the macro-scale computation. In [14], a sub-grid based model was suggested wherein a micro-scale model is applied for each sub-domain to pass information of volume fraction to the macro-scale model which is calculated based on the macro-scale temperature field. However, in these studies, no attempt is made to prove micro-macro thermodynamic balance laws when using the proposed scale transition. The emphasis in this paper, is to provide a generalized macro-micro homogenized model of diffusion problems with flux discontinuities where scale transitions are derived from balance laws.

Computational homogenization provides an attractive avenue for computing the macroscopic response in problems with discontinuities and non-linearities in the microstructural behavior. Application of such approaches for mechanical deformation has been well studied previously [16–19] and recently extended to thermomechanical problems [20]. In this approach, a representative volume element (RVE) is defined at the micro-scale and boundary conditions are defined on the RVE in terms of macroscopic quantities. The data from micro-scale simulations are used to extract quantities for the macroscopic simulation via consistent averaging schemes. Homogenization approaches remain valid as long as the length scale over which the macroscopic field variables vary remains much larger than the microscopic length-scale. Recently, such a scheme was developed for thermal conduction problems [21] using a well-behaved micro-scale model without flux discontinuities or moving interfaces. In this paper, computational homogenization approach has been developed for the case of fluid solidification problems. Macro-scale quantities such as heat flux are consistently computed from the microstructural sub-problem and heat flux discontinuity at the solidifying interface is handled during averaging through appropriate use of Stefan's condition. The convection-diffusion equation at the micro-scale is solved using enthalpy as the unknown variable to overcome difficulties arising from the presence of flux jump condition at the solid-liquid interface. Once the micro-scale problem is solved, the transport properties and fluxes are homogenized using consistent averaging schemes. The convergence behavior of the coupled macro-micro finite element scheme with respect to decreasing element size and time step is then analyzed by comparing with a known analytical solution. The paper is arranged as follows. In Sect. 2, the multi-scale formulation is introduced, followed by description of the micro- and macro-scale problems and the computational scheme in Sect. 3. In Sect. 4, we demonstrate the potential of the approach by comparing the results from this approach with a well-known analytical solution.

## 2 Multi-scale formulation

We consider a problem of heat conduction in an incompressible fluid, where parts of the fluid are frozen, while other parts are in a liquid state. The interface between the frozen and molten region is an unknown moving internal boundary. At the micro-scale, material 1 (in liquid state) occupies the domain $V^+$ and material 2 (in solid state) occupies the domain ($V^-$), where $V^+$ and $V^-$ are open subsets of $V$. At the interface $S^I$, material 2 solidifies further and advances into $V^+$. The interface $S^I$ moves in the direction $-\boldsymbol{n}^I$ with speed $V_n$, where $\boldsymbol{n}^I$ is the outward normal of $V^+$) at the interface.

Macro-micro linking is achieved by decomposing the micro-scale temperature field ($T$)into a sum of macroscopic field and a fluctuation field ($\tilde{T}$) as:

$$T = T_{\text{ref}} + \overline{\nabla T} \cdot \boldsymbol{x} + \tilde{T} \tag{1}$$

Here, $\boldsymbol{x}$ is the coordinate of a point on the micro-scale relative to a reference point on the bottom left corner of the microstructure where temperature is $T_{\text{ref}}$ (as shown in Fig. 1). In general, we denote a macroscopic counterpart of a microscopic field quantity (say, $\chi$) as $\overline{\chi}$. In the above equation,

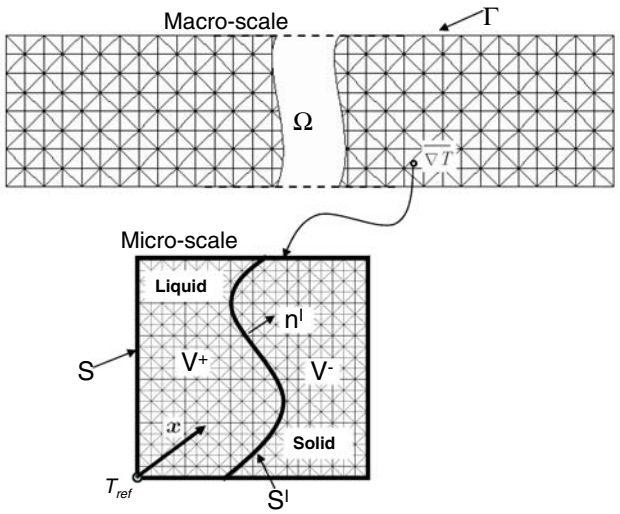


**Fig. 1** Multi-scaling procedure: Macro-scale is associated with a homogenized continuum. The macro-scale temperature (and gradient in temperature) is passed to the micro-scale as boundary conditions. Macro-scale quantities such as the thermal flux and conductivity (at the material point) are computed from the microstructural sub-problem through consistent averaging schemes

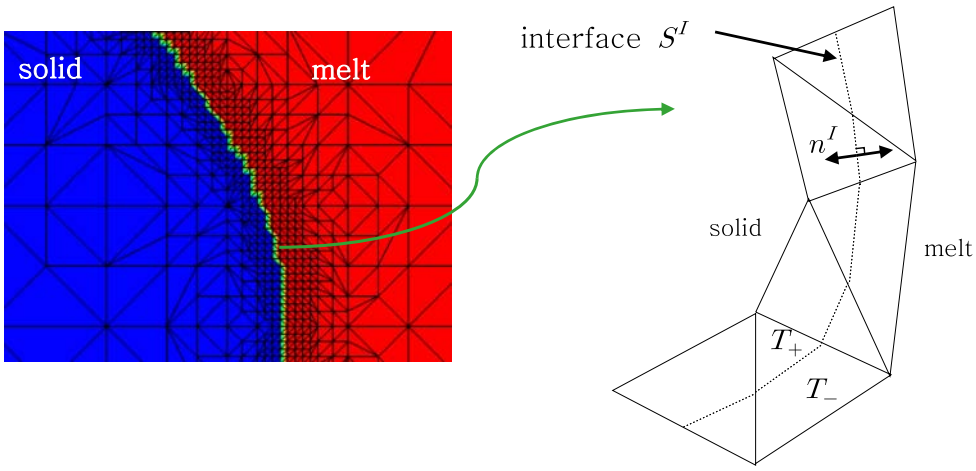


**Fig. 2** Solidifying interface is tracked using an adaptive meshing strategy. This allows flux discontinuities to be accurately modeled at the micro-scale

gradient in temperature at macroscopic material point is denoted as $\overline{\nabla T}$ ($= \nabla_{\text{macro}}\bar{T}$). Our basic homogenization assumption is that $\overline{\nabla T}$ can be computed from the temperature at the external boundary ($S$) of the microstructure with outward normal $\boldsymbol{n}$ as:

$$\overline{\nabla T} = \frac{1}{V}\int_S T\boldsymbol{n}\,dS \tag{2}$$

Using the decomposition of the micro-scale temperature field, it can be shown that:

$$\frac{1}{V}\int_V \nabla T dV = \overline{\nabla T} + \frac{1}{V}\int_V \nabla\tilde{T} dV \tag{3}$$

We employ the generalized divergence theorem of the form $\int_V \nabla\chi dV = \int_S \chi\boldsymbol{n}dS + \int_{S^I}[|\chi|]\boldsymbol{n}^I dS^I$ in the above equation (where, $[|\chi|]$ denotes the jump in the field quantity across the evolving interface ($S^I$) with normal $n^I$) to obtain the following relationship:

$$\frac{1}{V}\int_S T\boldsymbol{n}dS = \overline{\nabla T} + \frac{1}{V}\int_S \tilde{T}\boldsymbol{n}dS + \frac{1}{V}\int_{S^I}([|\tilde{T}|] - [|T|])\boldsymbol{n}^I dS^I \tag{4}$$

The jump in a field quantity, say $T$, across such an interface is computed as $[|T|] = T_+ - T_-$. Here, $T_+$ and $T_-$ refer to the quantity in domain $V^+$ and $V^-$, respectively, close to a point on the interface (as shown in Fig. 2). We aim to build boundary conditions at the micro-scale that satisfies Eq. 4. Assumption of $\tilde{T} = 0$ at all points in the microstructure leads to rule of mixtures (or Taylor model in deformation problems). This is not a valid assumption for solidification problems as the solid-melt interface is at the melting point, whereas in a Taylor model, temperature at all points are constrained as $T = T_{\text{ref}} + \overline{\nabla T}\cdot\boldsymbol{x}$. In addition, Taylor model solution does not satisfy micro-scale thermal equilibrium. Due to the strong constraint imposed on micro-scale temperatures, it can be shown that the Taylor model produces an upper-bound result for conductivities calculated. Two other boundary conditions are applicable to the solidification problem that can allow satisfaction of equilibrium constraint as well as interface temperature constraint. The first is an essential boundary condition on the surface of the microstructure and the other is a periodic boundary condition (refer [21]) on temperatures. In this paper, we restrict ourselves to the essential boundary conditions given below:

$$\tilde{T} = 0 \quad \text{on } S \tag{5}$$

$$([|\tilde{T}|] - [|T|]) = 0 \quad \text{on } S^I \tag{6}$$

In this case, temperature at the boundaries of the microstructure is derived from the macro-scale temperature field and temperature gradient as $T = T_{\text{ref}} + \overline{\nabla T}\cdot\boldsymbol{x}$. The interface temperature jump constraint (Eq. 6) is trivially satisfied (by computing jump from Eq. 1 and noting that macroscopic fields are assumed continuous). In solidification problems, temperature fields are continuous ($[|T|] = 0$) and an additional boundary condition is applied that enforces the interface to be at the melting point (or calculated using Gibbs–Thomson relation for dendritic growth simulations (e.g., [13]).

Solidification is modeled at the micro-scale using the convection-diffusion equation:

$$\frac{\partial(\rho cT)}{\partial t} + \nabla\cdot\boldsymbol{q} = -\nabla\cdot(\rho cT\boldsymbol{v}) \tag{7}$$

where, $\boldsymbol{q}$ represents the heat flux ($\boldsymbol{q} = -k\nabla T$, where $k$ is the thermal conductivity), $\rho$ denotes the density, $c$ is the heat capacity and $\boldsymbol{v}$ represents the velocity field. For simplicity, convective effects within the fluid are ignored and the velocity field is assumed to be non-zero only on the evolving solidification front. Since the microscopic length scale is considered to be much smaller than the scale of variation of the macroscopic temperature field, the micro-scale can be

assumed to be at steady state at any instant of the macroscopic (transient) evaluation [21]. The microscopic diffusion equation is then given as:

$$\nabla \cdot \boldsymbol{q} = -\nabla \cdot (\rho c T \boldsymbol{v}) \tag{8}$$

Consider the space of weighting functions, $\mathcal{V}$, given by

$$\mathcal{V} = \{\phi : \phi \in H^1 \text{ over } V, \phi = 0 \text{ on } S\} \tag{9}$$

and the space of trial functions, $\mathcal{L}$, given by

$$\mathcal{L} = \{T : T \in H^1 \text{ over } V^+ \cup V^-, T \text{ given on } S \cup S^I\} \tag{10}$$

Weak form of the above equation can be simplified as follows (where $\phi$ is the weighting function that is assumed to be continuous across the microstructure):

$$(\nabla\phi, \boldsymbol{q})_V = (v_n[|\rho c T|], \phi)_{S^I} + ([|q_n|], \phi)_{S^I} \tag{11}$$

In the above equation, the symbol $(.,.)$ represents the Euclidean inner product over the domain given by the subscript. To obtain the above mentioned weak form, we have assumed that the velocity at all points (aside from the points on the interface) are small (i.e., $\boldsymbol{v} = 0$ on $V^+ \cup V^-$). As described previously, the micro-scale model includes both heat capacity jump ($[|\rho c|]$) and flux jump ($[|\boldsymbol{q}|]$) in the normal direction across the solidifying interface. The velocity of the solid-liquid interface is governed by the heat flux jump through the classical Stefan equation:

$$([|q_n|] + v_n[|\rho c|]T) = 0 \tag{12}$$

$$\text{where, } T[|\rho c|] = L \text{ or } [|q_n|] = -v_n L \tag{13}$$

where, $L$ is the latent heat of phase transformation per unit volume.

Based on Stefan equation, it can be proved that the integral of normal heat flux over the microstructure surface goes to zero as follows:

$$\begin{aligned}\int_S q_n \, dS &= \int_S \boldsymbol{q} \cdot \boldsymbol{n} \, dS = \int_V \nabla \cdot \boldsymbol{q} \, dV - \int_{S^I} [|q_n|] \, dS^I \\ &= -\int_V \nabla \cdot (\rho c T \boldsymbol{v}) dV - \int_{S^I} [|q_n|] dS^I \\ &= -\int_{S^I} (v_n[|\rho c|]T + [|q_n|]) dS^I = 0\end{aligned} \tag{14}$$

The above relation is subsequently used for homogenization of the micro-scale flux. In particular, we are interested in obtaining a macroscopic flux that satisfies Hill's macro-homogeneity condition (which relates the macroscopic flux ($\bar{\boldsymbol{q}}$) with its microstructural counterpart ($\boldsymbol{q}$ [22]) as follows:

$$\overline{\nabla T} \cdot \bar{\boldsymbol{q}} = \overline{\nabla T \cdot \boldsymbol{q}} \tag{15}$$

Application of the governing equation (Eq. 8) changes the macro-homogeneity condition to the following form:

$$\begin{aligned}\overline{\nabla T} \cdot \bar{\boldsymbol{q}} = \overline{\nabla T \cdot \boldsymbol{q}} &= \frac{1}{V}\int_V (\nabla \cdot (T\boldsymbol{q}) - T\nabla \cdot \boldsymbol{q}) dV \\ &= \frac{1}{V}\int_S T q_n dS + \frac{1}{V}\int_{S^I} [|T q_n|] dS^I \\ &\quad + \frac{1}{V}\int_V T\nabla \cdot (\rho c T \boldsymbol{v}) dV\end{aligned} \tag{16}$$

We can reduce the first term in the above equation using the definition of micro-scale temperature (Eq. 1) and the homogeneous boundary conditions as:

$$\begin{aligned}\frac{1}{V}\int_S T q_n \, dS &= \frac{1}{V}\int_S [T_{\text{ref}} + \overline{\nabla T} \cdot \boldsymbol{x}] q_n \, dS \\ &= \overline{\nabla T} \cdot \frac{1}{V}\int_S \boldsymbol{x} q_n dS \quad \left(\text{using } \int_S q_n dS = 0\right)\end{aligned} \tag{17}$$

The second and third terms in Eq. 16 are again reduced using the generalized divergence theorem as:

$$\begin{aligned}&\frac{1}{V}\int_{S^I} [|T q_n|] \, dS^I + \frac{1}{V}\int_V T\nabla \cdot (\rho c T \boldsymbol{v}) \, dV \\ &= \frac{1}{V}\int_{S^I} [|T q_n|] \, dS^I + \frac{1}{V}\int_V \nabla \cdot (\rho c T^2 \boldsymbol{v}) \, dV \\ &\quad - \frac{1}{V}\int_V \nabla T \cdot (\rho c T \boldsymbol{v}) \, dV \\ &= \frac{1}{V}\int_{S^I} T[|q_n|] dS^I + \frac{1}{V}\int_{S^I} T^2[|\rho c|] v_n dS^I = 0\end{aligned} \tag{18}$$

In the above derivation, we use Stefan equation and the fact that the particle velocity is zero at all points in the material except the interface. Combining Eqs. (16–18), the macroscopic flux is obtained as:

$$\bar{\boldsymbol{q}} = \frac{1}{V}\int_S \boldsymbol{x} q_n \, dS \tag{19}$$

The above equation allows macroscopic heat flux to be computed from the normal flux at the boundaries of the microstructure similar to Eq. 2. Using Stefan equation, we can also show that the macroscopic heat flux thus computed corresponds to the volume averaged heat flux at the micro-scale (see Appendix A).

## 3 Evaluation of homogenized transport properties

The macroscopic diffusion equation is defined on a uniformly meshed domain ($\Omega$) on which solidification occurs. Boundaries of the macro-scale domain is denoted as $\Gamma$. Solidification is explicitly modeled at the micro-scale, while only heat conduction is modeled at the macro-scale using homogenized quantities as follows:

$$\frac{\partial \bar{H}}{\partial t} = -\nabla \cdot \bar{\boldsymbol{q}},\ T(\Gamma, t > 0) = \widehat{T},\ T(\Omega, t = 0) = T_0 \quad (20)$$

where, the macroscopic (homogenized) enthalpy ($\bar{H}$) is defined using microscopic volume averaged heat capacity ($\overline{\rho c}$) as follows:

$$\bar{H} = \overline{\rho c T + L\rho f} = \overline{\rho c}\bar{T} + L\overline{\rho f} \quad (21)$$

Here, $f$ is the volume fraction of liquid in the micro-scale, $L$ is the latent heat of solidification defined per unit mass. In the above equation, the enthalpy is defined using microscopic volume averaged heat capacity ($\overline{\rho c}$). This definition is consistent with the condition that stored energy at macro-scale is same as the average micro-scale stored energy [21]. The temperature boundary conditions at the micro-scale is completely defined once $T_{\text{ref}}$ for the next time step is computed using Eqs. 21 and 1 at the end of each time step of the simulation. Due to the use of an explicit scheme to calculate $T_{\text{ref}}$, smaller time steps at the macro-scale allow better satisfaction of balance of stored energy. In the numerical examples, we report the error between the macro- and micro-stored enthalpy at various material points to show that the balance of stored energy condition (Eq. 21) is indeed satisfied during homogenization.

To solve the non-linear macroscopic equation (Eq. 20), Galerkin finite element method is adopted and the weak form is solved in an incremental-iterative manner using the Newton–Raphson method. The $(\lambda + 1)$th Newton–Raphson step at time $(t + 1)$ involves solution of the system $\boldsymbol{K}\{\delta\bar{H}^{\lambda+1,t+1}\} = \boldsymbol{f}$, where the unknown vector in the above system is the increment in the enthalpy ($\delta\bar{H}^{\lambda+1,t+1}$). To understand the micro-scale quantities that are needed to create the system of equations, the Jacobian matrix and force vector for a finite element $e$ with shape functions $N_i$ occupying a volume $\Omega^e$ is expanded below:

$$\begin{aligned} K^e_{ij} &= \frac{1}{\Delta t}\int_{\Omega^e} N_i N_j d\Omega - \int_{\Omega^e} \bar{\boldsymbol{\kappa}}^{\lambda,t+1}\nabla N_i \cdot \nabla N_j d\Omega \\ f^e_j &= \int_{\Omega^e} \bar{\boldsymbol{q}}^{\lambda,t+1} \cdot \nabla N_j d\Omega \\ &\quad - \frac{1}{\Delta t}\int_{\Omega^e} (\bar{H}^{\lambda,t+1} - \bar{H}^t) N_j d\Omega \end{aligned} \quad (22)$$

From the above equations, it is seen that to solve the macro-scale equations, one requires the homogenized conductivity $\bar{\boldsymbol{\kappa}}$ to be defined at each integration point in the macro-scale as follows:

$$\delta\bar{\boldsymbol{q}}^{\lambda,t+1} = \bar{\boldsymbol{\kappa}}^{\lambda,t+1}\delta(\overline{\nabla H}) \quad (23)$$

The homogenized conductivity can either be obtained using perturbation analysis [23] or by directly manipulating the converged Jacobian and residual matrices of the micro-scale problem [21]. In the former approach, each component of the macroscopic temperature gradient is independently perturbed by a small amount $\epsilon$ which affects the boundary conditions at the micro-scale through Eq. 1. The micro-scale problem is solved again using the perturbed boundary conditions and the resulting perturbation in homogenized flux is used to compute the homogenized conductivity. This involves solution of $N$ different micro-scale problems during each Newton–Raphson iteration at the macro-scale, where $N$ is the dimensionality of the macro-scale problem. Note that numerical approximation of the homogenized conductivity does not change the physical result in any way, only the speed of iteration process changes.

In this work, we follow the approach of [21] to obtain homogenized conductivity by direct manipulation of the converged Jacobian and residual matrices of the micro-scale problem. The steps to compute the homogenized conductivity using the approach is as follows. Macroscopic flux is first written using the vector of normal fluxes on the external nodes of the microstructure ($\{q_n^{\text{ext}}\}$) using finite element matrix representation as follows:

$$\overline{\boldsymbol{q}} = \frac{1}{V}\int_S \boldsymbol{x} q_n dS = \boldsymbol{L}\{q_n^{\text{ext}}\} \quad (24)$$

To compute the homogenized conductivity, one needs to compute sensitivity of $\{q_n^{\text{ext}}\}$ to perturbations in the macroscopic enthalpy gradient $\delta(\overline{\nabla H})$ as:

$$\delta\overline{\boldsymbol{q}} = \boldsymbol{L}\{\delta q_n^{\text{ext}}\} = \bar{\boldsymbol{\kappa}}\delta(\overline{\nabla H}) \quad (25)$$

To obtain the homogenized conductivity, the converged finite element solution from the Newton–Raphson iterations at the micro-scale is employed as follows:

$$\begin{bmatrix} \boldsymbol{K}_{ee} & \boldsymbol{K}_{ei} \\ \boldsymbol{K}_{ie} & \boldsymbol{K}_{ii} \end{bmatrix} \begin{bmatrix} \delta\boldsymbol{H}^e \\ \delta\boldsymbol{H}^i \end{bmatrix} = \begin{bmatrix} 0 \\ 0 \end{bmatrix}$$

In the above equation, the assembled matrix ($\boldsymbol{K}$) on the left hand side is the Jacobian matrix of the Newton–Raphson iteration. The residual on the right hand side goes to zero since the micro-scale solution has converged. The assembled matrix ($\boldsymbol{K}$) is arranged such that the vectors $\delta\boldsymbol{H}^e$ and $\delta\boldsymbol{H}^i$ contain the enthalpies on the external and internal nodes of the microstructure, respectively. Sensitivity of enthalpy on external nodes of the micro-scale mesh to the perturbation in

**Table 1** Solution scheme for multiscale homogenization of solidification problems

(1) Initialize macro-scale model and assign a microstructure to every integration point. Initially, all the underlying microstructures are in liquid state with known conductivity
(2) Apply time increment $\Delta t$ to the macro-scale problem
(3) Iteration step:
  (3.1) Assemble the macroscopic stiffness matrix
  (3.2) Solve the macroscopic system and compute temperature and the temperature gradient at each integration point
  (3.3) Loop over all integration points
    (a) Transfer boundary conditions to micro-scale problem using Eqs. 1, 5
    (b) Assemble and solve the micro-scale problem
    (c) Calculate the macro-flux (Eq. 19) and the macro-conductivity (Eq. 27) using the micro-scale solution and store the data
  (3.4) Assemble the macroscopic residual vector
(4) Check convergence, if not converged go to step 3, otherwise go to step 2

the imposed macroscopic enthalpy gradient can be written using matrix $\boldsymbol{G}$ [computed from the boundary condition on the temperatures on the external nodes (Eq. 1)] as follows:

$$\{\delta \boldsymbol{H}^e\} = \boldsymbol{G}\{\delta \overline{\nabla H}\} \tag{26}$$

Substituting the above relation into the converged matrix equation at the micro-scale and taking the known quantities to the right hand side, we obtain the equation:

$$\begin{bmatrix} \boldsymbol{K}_{ee} & \boldsymbol{K}_{ei} \\ \boldsymbol{K}_{ie} & \boldsymbol{K}_{ii} \end{bmatrix} \begin{bmatrix} 0 \\ \delta \boldsymbol{H}^i \end{bmatrix} = \begin{bmatrix} -\boldsymbol{K}_{ee}\boldsymbol{G}\delta\overline{\nabla H} \\ -\boldsymbol{K}_{ie}\boldsymbol{G}\delta\overline{\nabla H} \end{bmatrix}$$

The vector on the right hand side provides the sensitivity of microscopic flux to the macroscopic enthalpy gradient, which leads to the homogenized conductivity, $\bar{\boldsymbol{\kappa}}$ as follows:

$$\begin{aligned} \delta q_n^{ext} &= -\boldsymbol{K}_{ee}\boldsymbol{G}\delta\overline{\nabla H} \\ \bar{\boldsymbol{\kappa}} &= -\boldsymbol{L}\boldsymbol{K}_{ee}\boldsymbol{G} \end{aligned} \tag{27}$$

The overall solution scheme is shown in Table 1. To aid in speeding up the solution process for the multi-scale problem, the algorithm was parallelized using MPI. The macro-scale domain was decomposed and elements in each domain distributed to different processors. The underlying micro-scale problems were solved in serial within each processor. The simulator was developed using object oriented programming and was dynamically linked to the parallel toolbox PetSc [24] for parallel assembly and solution of linear systems. For solution of linear systems, a GMRES solver along with block Jacobi and ILU preconditioning was employed.

## 4 Numerical examples

In order to validate the multi-scale simulation procedure, a well-studied one-dimensional solidification problem is employed. In this simulation, one end of the simulation domain is fixed to a temperature less than melting point. The other end is assumed to at infinity and fixed to a temperature larger than the melting point so that the solid-liquid interface moves between these two ends. The analytic solution for the position of the interface ($X(t)$) at various times can be expressed as the following [25]:

$$X(t) = 2\lambda\sqrt{\alpha_s t} \tag{28}$$

In the above expression, $\alpha = (\frac{k}{\rho c})$ where $k$ is the thermal conductivity and the subscripts $s$ and $l$ are used when using properties of solid and liquid phase respectively. Constant $\lambda$ is equal to 0.2037 for this particular problem [26]. The analytical solution for the temperature history can be expressed as [25] (where $erf$ is the error function and $T_m = 0°\text{C}$ is the melting point for the fluid):

$$T = \begin{cases} T(0,t) + \frac{T_m - T(0,t)}{erf(\lambda)} erf\left(\frac{x}{2\sqrt{\alpha_s t}}\right) & x < X(t) \\ T_m & x = X(t) \\ T(\infty,t) + \frac{T_m - T(\infty,t)}{1 - erf\left(\lambda\sqrt{\frac{\alpha_s}{\alpha_l}}\right)} \left(1 - erf\left(\frac{x}{2\sqrt{\alpha_l t}}\right)\right) & x > X(t) \end{cases} \tag{29}$$

In the numerical simulations, the problem is modeled in a two-dimensional domain discretized using three-noded triangular elements at the macro- and micro-scales. A sufficiently large FE model size is chosen to approximate the infinite boundary. The material properties, boundary conditions, and initial conditions for the material used in this simulation are provided in the Table 2.

### 4.1 Micro-scale simulation approach

The problem is addressed using a single scale model as well as a multi-scale model to validate the results. Solution of micro-scale problem presents computational difficulties due to the presence of interface conditions in the form of an essential boundary condition and specified heat flux jump.

**Table 2** List of material constants (for both solid and liquid phase) and boundary and initial conditions used for the 1D solidification problem

| Material constant | Value |
|---|---|
| $L$ (kJ/kg) | 100,000 |
| $\rho$ (kg/m$^3$) | 1 |
| $c$ (kJ/kgK) | 2,500 |
| $k$ (W/mK) | 2 |
| BC's | IC's |
| $\begin{cases} T(x=0,y,t)=-4°\text{C} \\ T(x=\infty,y,t)=2°\text{C} \end{cases}$ | $\begin{cases} T(x=0,y,0)=-4°\text{C} \\ T(x>0,y,0)=2°\text{C} \end{cases}$ |

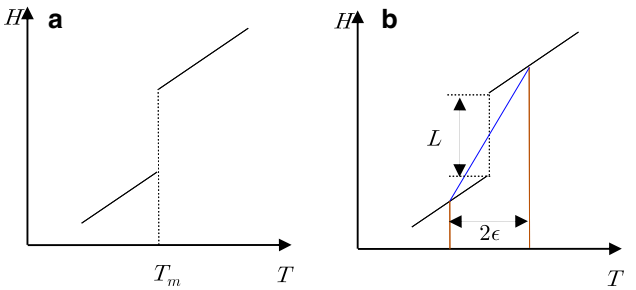


**Fig. 3** Schematic of the enthalpy-temperature relationship for a pure substance; **a** H is a discontinuous function of the temperature. **b** Numerical treatment of discontinuity [27]

To overcome these issues, we have employed the now well-established enthalpy formulation [27] to solve the micro-scale problem. Using the enthalpy formulation, it is possible to formulate a solution procedure where the flux jump condition is automatically satisfied without explicitly tracking the internal boundary. The governing equation is posed using enthalpy as the unknown variable and the equations are solved using a standard Galerkin FE formulation. Enthalpy is a discontinuous function at the interface as latent heat is added during phase change from solid to liquid state. In the enthalpy approach, the discontinuity of enthalpy at the interface is treated by allowing it to be continuous in a small region with $T_s = T_m - \epsilon$ and $T_l = T_m + \epsilon$ around the interface as shown in Fig. 3. Because of this numerical treatment, the desired interface behavior can be achieved without divergence and singularity issues. In particular, the following enthalpy function with respect to temperature has been used in this work (with $\epsilon = 0.1K$):

$$H = \begin{cases} \rho cT & T < T_s \\ \rho cT_s + \rho\left(\frac{2c\epsilon+L}{2\epsilon}\right)(T - T_s) & T_s \le T < T_l \\ \rho cT + \rho L & T > T_l \end{cases} \tag{30}$$

## 4.2 Case 1. Single-scale simulation results

We first compare simulation results (based on the enthalpy formulation) to the analytical solution. Please note that the simulation reported in this case is a *transient* simulation

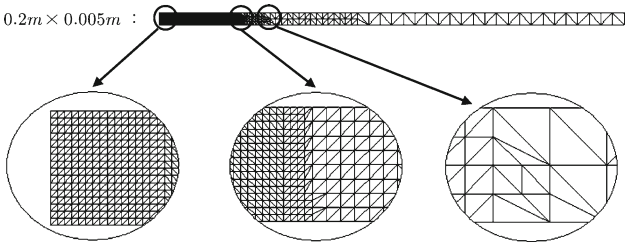


**Fig. 4** Case 1 study: finite element model for single-scale simulation uses adaptive grids with refinement in the region of the moving interface

based on Eq. 7. Adaptive meshing is employed with grids continuously refined in the region of the interface during the simulation in order to accurately track the solidification front as shown in Fig. 4. The interface velocities (solidification front) and the temperature distribution is well predicted by the model and compares favorably with the analytic solution. Comparison of numerical results with the analytical solution of the solidification front position and temperature time history at various locations is shown in Fig. 5a, b respectively.

## 4.3 Case 2. Multi-scale simulation

In the multi-scale simulation reported here, the micro-scale is considered to be in steady state as given in Eq. 8 while the time-dependence is incorporated at the macro-scale using Eq. 20. The finite element model at the microscopic scale for the multi-scale simulation is shown in Fig. 6.

The ability of the multi-scale model to capture the solidification front accurately is dictated by the mesh density at the macro-scale. Two meshes with increasing mesh density were used to test the convergence behavior of the multi-scale model. These meshes are depicted in Fig. 7.

Due to the tightly coupled nature of the macro- and micro-scale problems, numerical convergence needs to be established through careful control of mesh size and time steps. In all cases, the time steps were carefully controlled so that difference in enthalpy at the macro- and micro-scales at various integration points are minimized. As discussed in Sect. 3, energy balance dictates the choice of time steps used in the multi-scale problem. In order to ascertain the time step size needed to solve the multi-scale problem, the enthalpy difference between macro- and micro- at the integration points is computed as below:

$$\text{Mean square error} = \sqrt{\frac{\sum\left(\frac{H_M^i - \bar{H}^i}{H_M^i}\right)^2}{N}} \tag{31}$$

In the above equation, $H_M$ denotes the macro-scale enthalpy, $\bar{H} = \frac{1}{V}\int_V H dV$ is the volume average of enthalpy ($H$) at the micro-scale and $N$ denotes number of integration points in macro-scale FE model. As shown in the Fig. 8a, the error

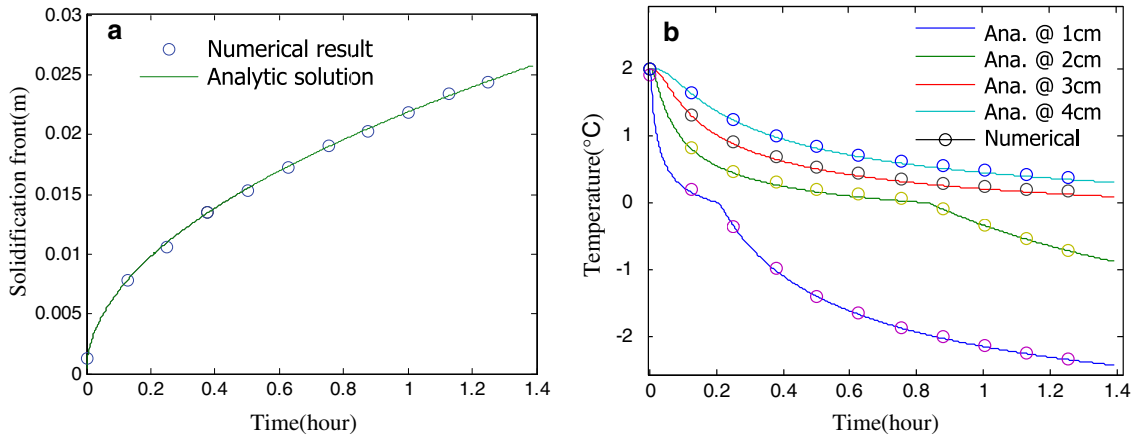


**Fig. 5** **a** Position of the phase change interface versus time in single-scale simulation. **b** Comparison of numerical and analytic solution of temperature history at $x = 1, 2, 3$ and 4 cms.

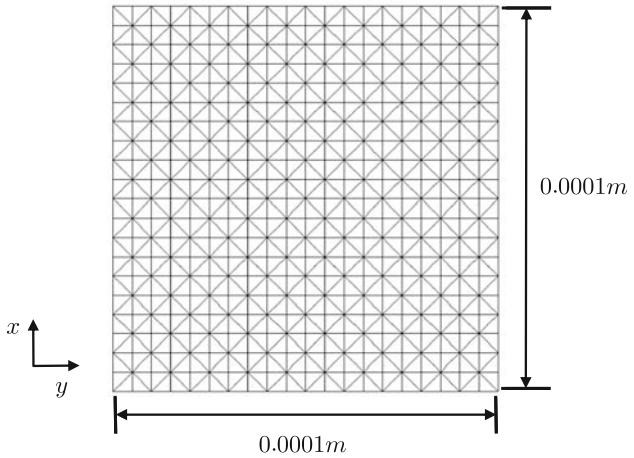


**Fig. 6** Finite element mesh used in the micro level

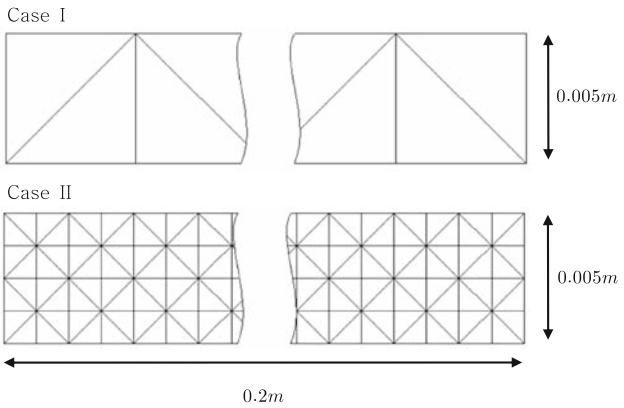


**Fig. 7** Two FE models at the macro-level with different mesh sizes are used in order to test convergence of the multi-scale simulation result

increases rapidly as time step, $\triangle t$ increases beyond 8 seconds for Case I. If a time step larger than 8 seconds is employed, the simulation rapidly diverges during the non-linear iterations. It is seen that the choice of time step is closely related to the mesh density used at the macro-scale. The overall error in enthalpy remains the same as the time step is reduced below eight seconds. The percentage error at each integration point calculated as $100(\frac{H_M^i - \bar{H}^i}{H_M^i})$ is plotted in Fig. 9a, b for the coarse and fine macro-scale mesh, respectively. The enthalpy difference between micro- and macro-scales are primarily observed at elements that involve the evolving interface due to a large jump in enthalpy at these locations.

During homogenization, the front is not as accurately tracked as in a single scale simulation (where adaptive meshing was used to capture the interface details). It is to be noted that the aim of homogenization is to obtain a homogenized description of the interface and capture fine scale information at various points in the macro-mesh with lower computational effort. The accuracy obtained during tracking of the solid-liquid interface is dictated by the element size in the macro-scale mesh. As the element size reduces, it is expected that the interface is better represented in the macro-scale model. As expected, it is seen from Fig. 9b that the enthalpy errors between macro- and micro-scales decreases as FE model with a finer macro-scale grid (Case II). A time step of one second was used in this case based on the mean square enthalpy error tests plotted in Fig. 8b.

The results of solidification front position and the temperature-time history at various locations in the mesh are compared with analytical solution for two cases in Figs. 10 and 11 respectively. It is clear that as finer grids are employed at the macro-scale, the solid-liquid interface and temperature distribution are captured in an increasingly better manner. Multi-scale approach proposed here is computationally well suited in problems where there is a clear scale separation (e.g., dendritic microstructure formation) and it is computationally impossible to resolve the fine scale details at macroscopic scales. Although the problem chosen here mimics

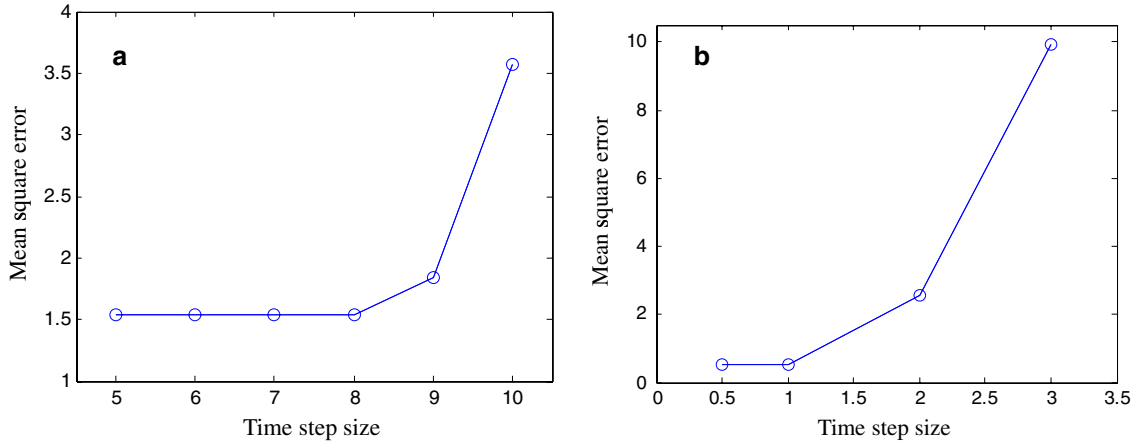


**Fig. 8** Mean square enthalpy errors with respect to time step size (in seconds) for the two cases. The errors are computed during the simulation from $t = 4995\,\mathrm{s}$ to $t = 4995\,\mathrm{s} + \triangle t$. (**a**) Case I—total number of element : 80. (**b**) Case II—total number of element : 1280

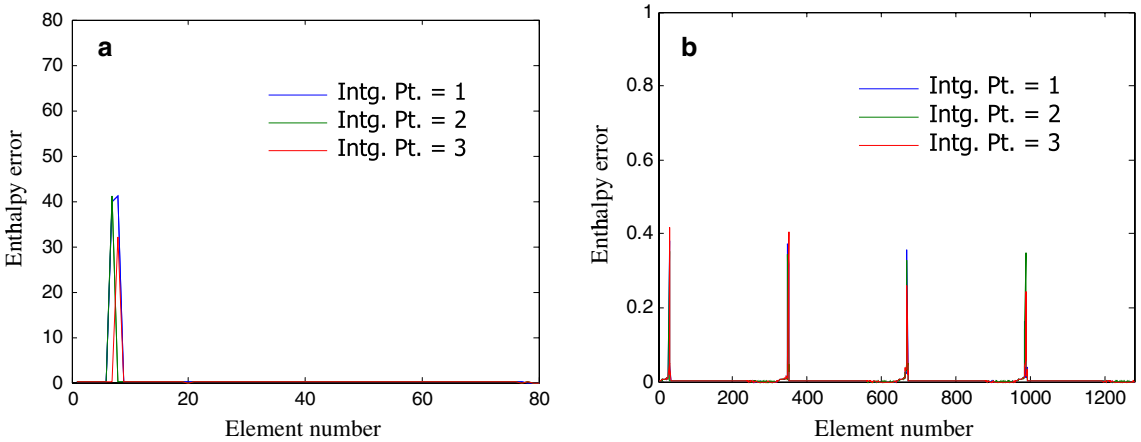


**Fig. 9** The enthalpy errors (in %) on each of the three integration points for all macro-scale elements at a simulation time of $t = 2{,}500\,\mathrm{s}$. **a** Case-I: elements along the $x$-axis in the macroscopic FE model are ordered from left to right. **b** Case-II: the enthalpy error for all elements are shown, there are four rows of elements along $y$-axis (see Fig. 7b), leading to four peaks for elements located at the interface

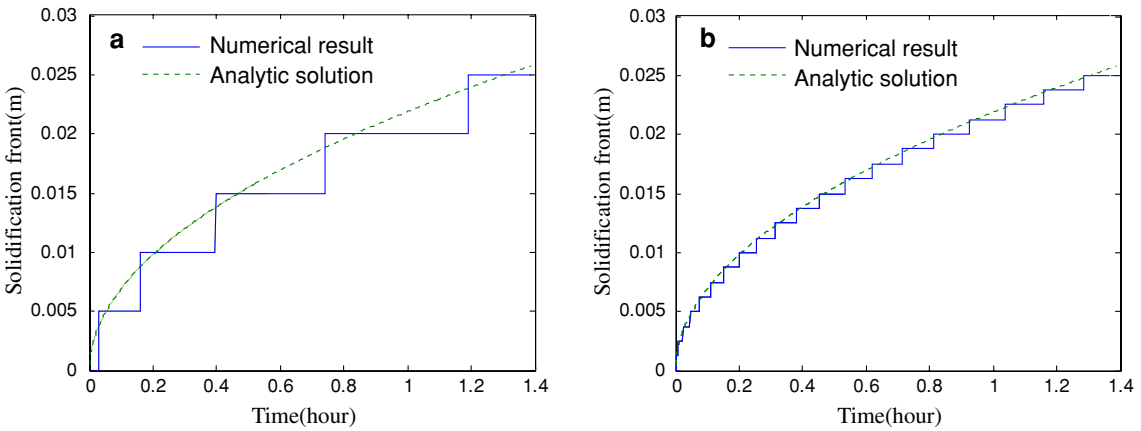


**Fig. 10** Comparison of predicted and analytical solution for interface positions computed using FE mesh from **a** case I, **b** case II. During homogenization, the true location of the interface is not explicitly tracked in the macro-scale. The elements where the interface is located are depicted in the figure

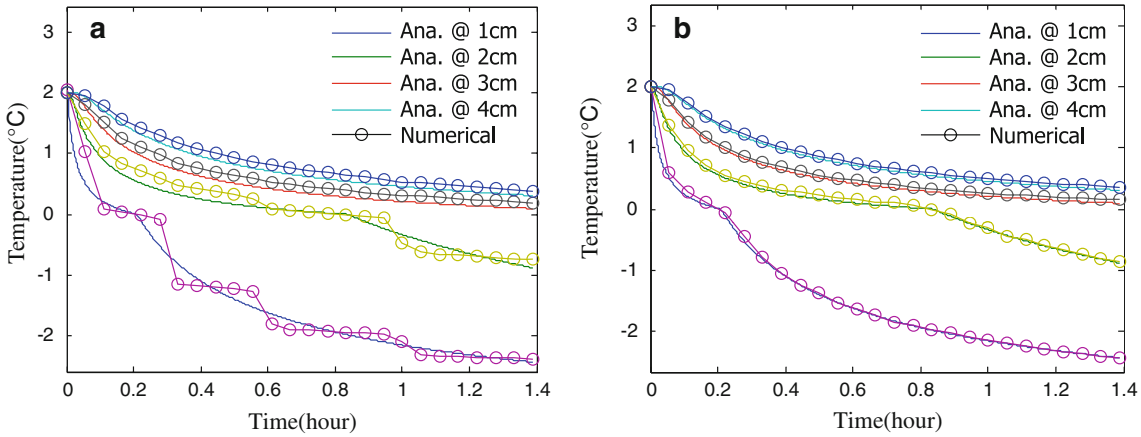


**Fig. 11** Comparison of predicted and analytical solution of temperature history at four different locations in the macro-scale mesh for **a** case I, **b** case II

scale separation, the real purpose however, is to validate the multi-scale homogenization with a known analytical solution. Future work in this area would involve development of adaptive mesh refinement and time-stepping methods to accelerate computation and address problems with large scale separation.

## 5 Conclusion

In this paper, a non-linear coupled macro-micro finite element model is presented for addressing fluid solidification problems. Solidification problems involve evolution of surfaces coupled with flux jump boundary conditions across interfaces that have not been addressed using homogenization approaches. Homogenization of complex micro-scale behavior including moving interfaces and flux jumps has been performed. Based on the Hill's macro-homogeneity condition, macroscopic quantities are evaluated via consistent averaging of the microscopic values. The micro-scale model incorporates the physics associated with solidification including moving interfaces and flux discontinuities, while the macro-scale model needs to only model thermal conduction using continuous (homogenized) fields. The convergence behavior of the coupled macro-micro finite element scheme with respect to decreasing element size is analyzed by comparing with a known analytical solution of the Stefan problem. In this coupled non-linear multi-scale problem, although good convergence is achieved at higher mesh densities, the time steps need to be carefully controlled to achieve macro-micro enthalpy balance and numerical stability. The approach is expected to be computationally superior in problems where there is a large scale separation between micro and macro scales, e.g., in case of dendritic growth.

**Acknowledgments** This work was sponsored by NASA Constellation University Institutes Project under grant NCC3-989 with Claudia Meyer as the project manager.

## Appendix A: Volume average of heat flux at the micro-scale

Using the governing equation at the micro-scale (Eq. 8), we obtain the expression for $\nabla \cdot \boldsymbol{xq}$ as:

$$\nabla \cdot (\boldsymbol{xq}) = \boldsymbol{q} + \boldsymbol{x}\nabla \cdot \boldsymbol{q} = \boldsymbol{q} - \boldsymbol{x}\nabla \cdot (\rho c T \boldsymbol{v})$$

Using the above equation and application of the generalized divergence theorem, we can obtain the volume average of heat flux as:

$$\begin{aligned}\frac{1}{V}\int \boldsymbol{q} dV &= \frac{1}{V}\int_V (\nabla \cdot (\boldsymbol{xq}) + \boldsymbol{x}\nabla \cdot (\rho c T \boldsymbol{v}))dV \\ &= \frac{1}{V}\int_S \boldsymbol{x} q_n dS + \frac{1}{V}\int_{S^I} \boldsymbol{x}[|q_n|]dS^I \\ &\quad + \frac{1}{V}\int_V \boldsymbol{x}\nabla \cdot (\rho c T \boldsymbol{v})dV\end{aligned}$$

The last term in the above equation can be rewritten as:

$$\begin{aligned}\frac{1}{V}\int_V \boldsymbol{x}\nabla \cdot (\rho c T \boldsymbol{v})dV &= \frac{1}{V}\int_V \nabla \cdot (\rho c T \boldsymbol{x} \otimes \boldsymbol{v})dV \\ &\quad - \frac{1}{V}\int_V \rho c T \boldsymbol{v} dV \\ &= \frac{1}{V}\int_{S^I} \boldsymbol{x}[|\rho c|]T v_n dS^I\end{aligned}$$

In the above derivation, we have used the fact that particle velocity is zero at all points in the domain except at the interface to eliminate the terms involving volume integral of velocity. The above equation can be used to obtain the expression for volume average of heat flux as:

$$\frac{1}{V}\int \boldsymbol{q}dV = \frac{1}{V}\int_S \boldsymbol{x}q_n dS + \frac{1}{V}\int_{S^I} \boldsymbol{x}([|q_n|]+[|\rho c|]Tv_n)dS^I$$
$$= \frac{1}{V}\int_S \boldsymbol{x}q_n dS$$

As a consequence of this derivation, we prove that the volume averaged heat flux can be obtained using information on the boundary of the microstructure.

## References


1. Hashin Z (1983) Analysis of composite materials. J Appl Mech 50:481–505
2. Rosen BW, Hashin Z (1970) Effective thermal expansion coefficients and specific heats of composite materials. Int J Eng Sci 8:157–173
3. Noor AK, Shah RS (1993) Effective thermoelastic and thermal properties of unidirectional fiber-reinforced composites and their sensitivity coefficients. Comput Struct 26:7–23
4. Auriault JL (1983) Effective macroscopic description of heat conduction in periodic composites. Int J Heat Mass Transf 26(6): 861–869
5. Boutin C (1995) Microstructural influence on heat conduction. Int J Heat Mass Transf 38(17):3181–3195
6. Guedes JM, Kikuchi N (1990) Preprocessing and postprocessing for materials based on the homogenization method with adaptive finite element methods. Comput Methods Appl Mech Eng 83: 143–198
7. Jiang M, Jasiuk I, Ostoja-Starzewski M (2002) Apparent thermal conductivity of periodic two-dimensional composites. Comput Mater Sci 25:329–338
8. Ostoja-Starzewski M, Schulte J (1996) Bounding of effective thermal conductivities of multiscale materials by essential and natural boundary conditions. Phys Rev B 54(1):278–285
9. Sigmund O, Torquato S (1997) Design of materials with extreme thermal expansion using a three-phase topology optimization. J Mech Phys Solids 45:1037–1067
10. Wang CY, Beckermann C (1995) Equiaxed dendritic solidification with convection: part I. Multiscale/Multiphase modeling. Metallurgical Mater Trans A 25:2754–2764
11. Eck C, Knabner P, Korotov S (2002) A two-scale method for the computation of solid-liquid phase transitions with dendritic microstructure. J Comput Phys 178:58–80
12. Lee PD, Chirazi A, Atwood RC, Wang W (2004) Multiscale modelling of solidification microstructures, including microsegregation and microporosity, in an Al-Si-Cu alloy. Mater Sci Eng A 365: 57–65
13. Tan L, Zabaras N (2007) Multiscale modeling of alloy solidification using a database approach. J Comput Phys 227:728–754
14. Rafii-Tabar H, Chirazi A (2002) Multiscale computational modelling of solidification phenomena. Phys Rep 365:145–249
15. Gravemeier V, Lenz S, Wall WA (2008) Towards a taxonomy for multiscale methods in computational mechanics: building blocks of existing methods. Comput Mech 41:279–291
16. Smit RJM, Brekelmans WAM, Meijer HEH (1998) Prediction of the mechanical behaviour of nonlinear heterogeneous systems by multi-level finite element modeling. Comput Methods Appl Mech Eng 155:181–192
17. Miehe C, Schroeder J, Schotte J (1999) Computational homogenization analysis in finite plasticity. Simulation of texture development in polycrystalline materials. Comput Methods Appl Mech Eng 171:387–418
18. Kouznetsova VG, Brekelmans WAM, Baaijens FPT (2001) An approach to micromacro modeling of heterogeneous materials. Comput Mech 27:37–48
19. Sundararaghavan V, Zabaras N (2006) Design of microstructure-sensitive properties in elasto-viscoplastic polycrystals using multi-scale homogenization. Int J Plast 22:1799–1824
20. Ozdemir I, Brekelmans WAM, Geers MGD (2008) $FE^2$ computational homogenization for the thermo-mechanical analysis of heterogeneous solids. Comput Methods Appl Mech Eng 198(3–4): 602–613
21. Ozdemir I, Brekelmans WAM, Geers MGD (2008) Computational homogenization for heat conduction in heterogeneous solids. Int J Numer Meth Eng 73:185–204
22. Ostoja-Starzewski M (2002) Towards stochastic continuum thermodynamics. J Non Equilib Thermodyn 27:335–348
23. Miehe C (1996) Numerical computation of algorithmic (consistent) tangent moduli in large-strain computational inelasticity. Comput Meth Appl Mech Eng 134(3–4):223–240
24. Balay S, Buschelman K, Eijkhout V, Gropp WD, Kaushik D, Knepley MG, McInnes LC, Smith BF, Zhang H (2004) PETSc users manual ANL-95/11—revision 2.1.5. Argonne National Laboratory
25. Rubenstein LI (1971) The Stefan problem. Trans Math Monographs. American Mathematical Society (AMS), Providence, p 27
26. Crank J (1984) Free and moving bounday problems. Clarendon Press, Oxford
27. Shyy W, Udayhumar HS, Rao MM, Smith RW (2007) Computational fluid dynamics with moving boundaries, 1st edn. Dover, Mineola